Chapter 5

Near Infrared (NIR) Camera Facility

5.1 Introduction

One of the important requirements of iRobo-AO is for it to be able to work in visible as well as in Near Infrared regimes. We developed the Near Infrared (NIR) camera at IUCAA to integrate with iRobo-AO, to improve its scientific abilities. It is capable of providing high-angular resolution, low noise, wide angle field of view ($\approx 1.0'$), and high-sensitivity in the near-infrared regime with unprecedented observing efficiency. It will provide iRobo-AO with an additional channel to do real time tip-tilt correction while science observation is being done simultaneously.

The NIR camera has a focal reducer, which was designed[106, 107] to accommodate the entire $\approx 1.0'$ diameter AO-corrected field within a detector of 1k $\times$ 1k pixels in size[1]. It is mounted at the AO corrected NIR focus of iRobo-AO (Fig 2.4, 5.1). The FOV at EMCCD and the NIR camera are not identical as the AO correction provides larger sky coverage for longer wavelength. It is possible to use EMCCD and the NIR camera simultaneously. In default mode, either EMCCD or NIR camera will be used for tip/tilt measurement. However, if both are used for science, Lucky imaging[18, 80] can be used for offline tip-tilt correction.

[1]It is an H2RG detector with 2k $\times$ 2k pixels, out of which only 1k $\times$ 1k is science grade. Teledyne does not make 1k x 1k sensors routinely anymore and a special order would have had a long lead time for delivery.

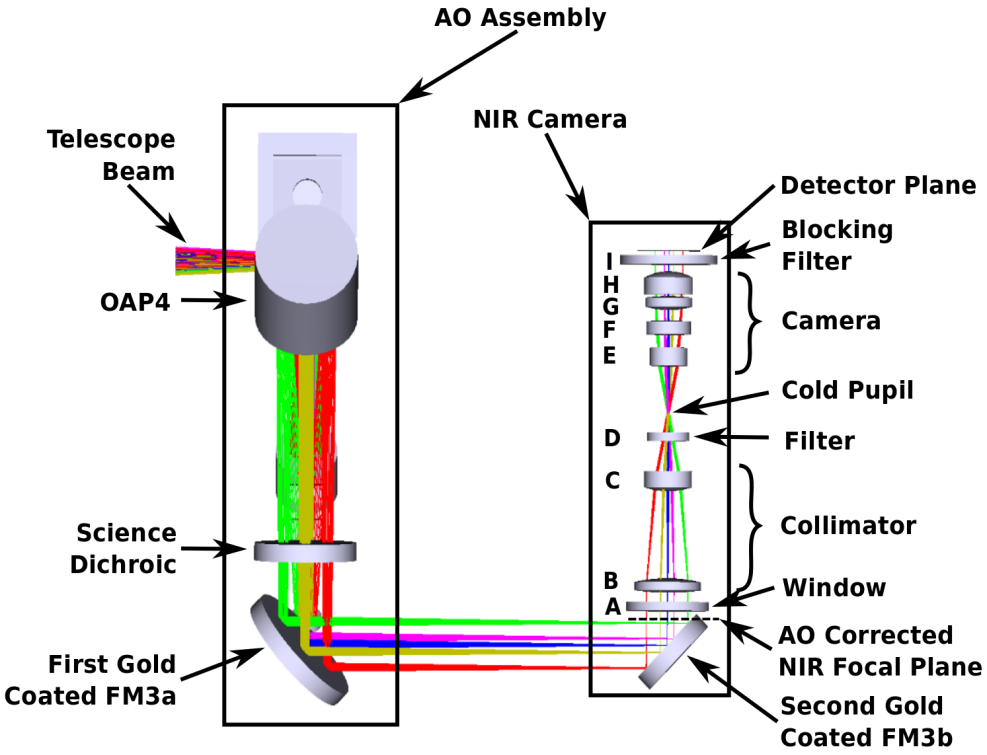

FIGURE 5.1: Optical layout of NIR camera and its position in iRobo-AO.

In this chapter, we briefly mention the features of the NIR camera. The entire chapter is organized as follows. Section 5.2 describes the optical architecture of NIR Camera. Section 5.3 describes various features of NIR Camera such as various chambers, radiation shield, cooling system, filter wheel mechanism etc. Thermal analysis and the cryogenic system are explained in section 5.4. Detector control system is presented in section 5.5.

5.2 NIR Camera Optical Architecture and Performance

A dichroic filter called science dichroic, mounted close to Off-Axis Parabolic mirror 4 (OAP4) (Fig.5.1, 2.4) transmits the NIR beam to the first gold coated mirror and reflects the visible part of the incoming light towards an Electron Multiplying CCD camera. The first gold-coated mirror steers the NIR light out from the iRobo-AO assembly box. The folded beam is again reflected from a second gold-coated mirror (FM3b) and finally enters the NIR camera (shown in Fig. 5.1).

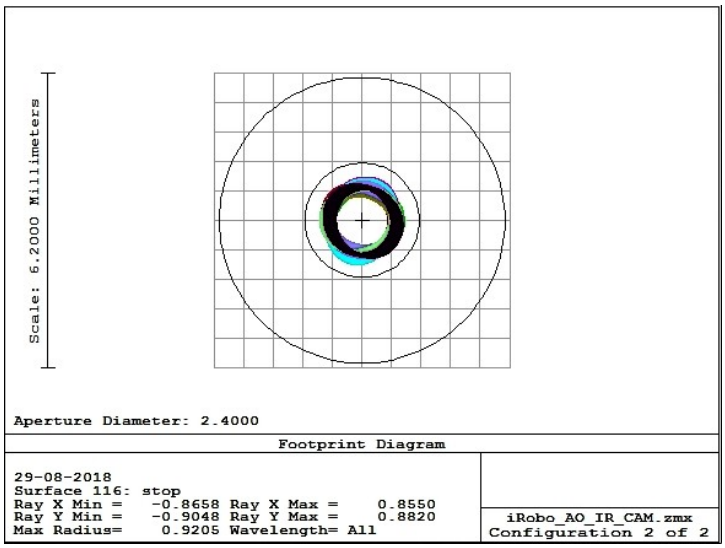

FIGURE 5.2: NIR camera pupil: actual size 1.9 mm, the solid circle represents the cold stop of 2.4 mm diameter clear aperture.

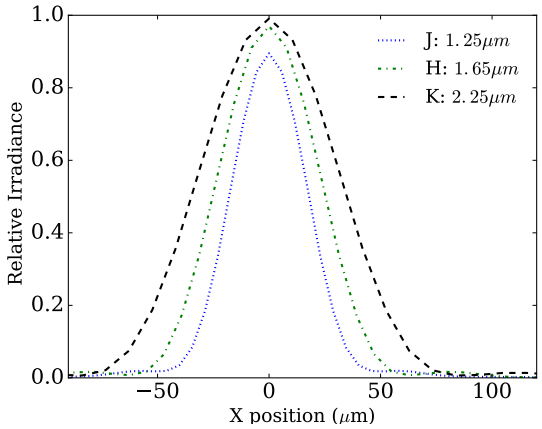

FIGURE 5.3: PSF, FWHM of PSFs in, J filter: 39 μm (=2.16 pixel), H filters: 51.77 μm (=2.87 pixel) and K filter: 70.14 μm(=3.9 pixel), satisfies Nyquist Criteria in all bands.

The window glass (A) is made of NIR grade fused silica. The input beam from iRobo-AO NIR focus is first collimated by the collimator (lenses B and C) which forms a pupil with a diameter of about 1.9 mm.

A cold stop made of thin copper foil and having a clear aperture of 2.4 mm is mounted at the pupil plane. The pupil size is optimized as a trade-off between stray light contamination and pupil vignetting due to flexures, misalignments etc. The displacement of the pupil under its gravity is very negligible ($\sim 0.2\mu m$) as per FEA analysis.

A filter wheel is mounted in the path of the collimated beam just before the cold

TABLE 5.1: Optical Features.

Parameters	Description
Field of view	Optical design is optimized over 1.2′ diameter
Elements (all are singlet)	No of elements for collimator and camera are 2 and 4 respectively. (all are singlet)
Window glass	5 mm thick Fused Silica
Length of NIR optics	≈ 212 mm (excluding dewar cooling system)
Output $f_{\#}$	30.76 (at detector)
Demagnification	∼ 1.5
Plate Scale	$3.37''/mm$
Sampling (λ : 1.6 μm)	FWHM of the spot at 1.6 μm wavelength is 50.6 μm, 2.8 pixels
Pupil Size	2.4 mm, optimized over given field, it cuts the stray light (Fig. 5.2)
Number of gold-coated mirrors	2, to fold the light
Filters	J, H, K, K_s, K′ at filter wheel, one blocking band pass (1-2.5 μm) filter
NIR Lens Material	Standard IR glasses (Table no 5.2)

stop, which at present carries J, H, K′ and Ks band one inch diameter filters, as well as a Dark. These NIR filters are very close to the pupil. Any impact of nonuniformity in the filter will be calibrated during commissioning.

The imaging camera of the focal reducer consists of four lenses (E to H in Fig. 5.1)which converts the input f/45.61 beam to an f/30.76 output beam. The camera accommodates the entire AO corrected 1.0′ diameter FOV across the 1k×1k detector. The image spot sizes satisfy the Nyquist sampling criteria for 18 micron pixel size of the detector. The entire optics is housed inside a vacuum cryogenic dewar. The optics are maintained at a temperature of $-100°C$. An IR blocking filter which has more than 97% transmissivity between 1.025 - 2.475 μm (less than 1% between 0.080-0.975 μm and less than 0.1% between 2.525-2.540 μm) is mounted close to the detector. There are several components of the optical train after the cold pupil. While they are cold, there will still be NIR emission from these components that will increase the background. The H2RG has around 5% QE at the 2.5 μm. The IR-blocking filter suppresses this contamination and leaks through the NIR filter to acceptable levels. This filter blocks any stray radiation beyond our working wavelength range from reaching the detector. Thermal analysis of the design performed using Zemax optical design software at two environment conditions ($-100°C$, 0 ATM and $20°C$, 1 ATM) satisfy all user constraints; the two environment conditions being chosen to simulate the working and fabrication environments respectively.

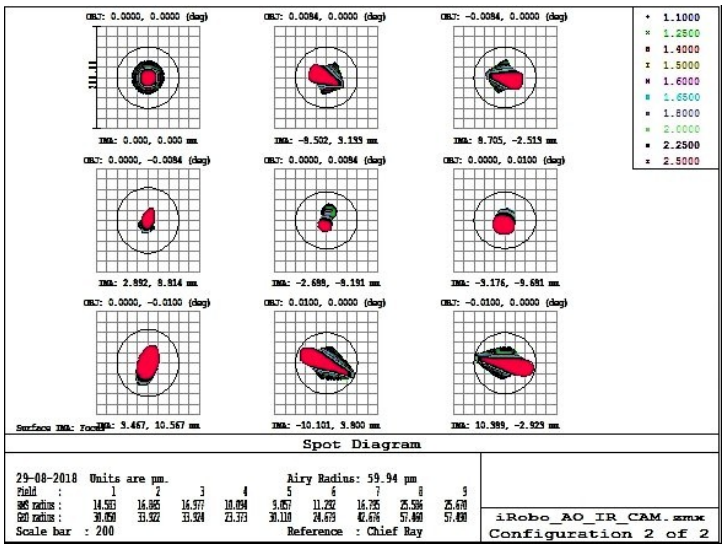

FIGURE 5.4: Spot Diagram: well within 60 μm Airy disc radius (at primary wavelength 1.6 μm) at different field points over 1.2′ diameter FOV, at -100^{o}C and 0 ATM.

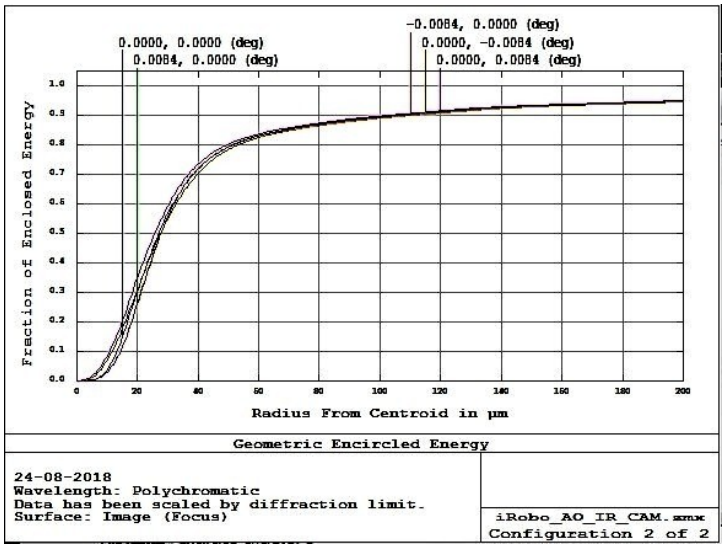

FIGURE 5.5: Encircled Energy: 80% energy is encircled within 60 μm radius of Airy Disc, at primary wavelength, over 1.2′ diameter FOV, at -100^{o}C and 0 ATM.

TABLE 5.2: Lens Prescription(@20^{o}C, 1 ATM Pressure).

Index†	Name	Material	Thickness (mm)	Radius1 ‡ (mm)	Radius2 ‡ (mm)	Diameter (mm)
A	Window	F_SILICA	5	Infinity	Infinity	51
B	Collimator 1st Lens	CAF2	8.12407	175.75639	-93.86728	41
C	Collimator 2nd Lens	ZNS_BROAD	10.05962	48.55256	86.50649	29.4
D	Filter	F_SILICA	5	Infinity	Infinity	25.4
E	Camera 1st Lens	ZNS_BROAD	11.00918	124.13349	-199.77275	23
F	Camera 2ns Lens	F_SILICA	8.3626	153.38423	-313.53429	27.4
G	Camera 3rd Lens	CAF2	8.01679	55.30077	-98.62260	29
H	Camera 4th Lens	F_SILICA	7.9948	-24.70975	-32.75707	30
I	Blocking Filter	F_SILICA	5	Infinity	Infinity	60

† The alphabetical index of the component are mentioned in Fig 5.1 for identification.
‡ The radius of curvature of the incident and exit surface of lens are Radius1 and Radius2 respectively.

TABLE 5.3: Specification of filters used in.

Index	Name	Position	Central Wavelength	Bandwidth $\Delta\lambda$
1	Dark*	1	- - -	- - -
2	J	2	1.25 μm	0.3 μm
3	H	3	1.65 μm	0.3 μm
4	K	4	2.2 μm	0.4 μm
5	K′	5	2.12 μm	0.34 μm
6	Ks	6	2.15 μm	0.32 μm

*It is a cold metal piece, which blocks all NIR photons for taking dark frames.

Optical features of the NIR camera design, lens and filter specifications are presented in Table 5.1, Table 5.2 and in Table 5.3. Optical performance of the design are discussed below.

The Point Spread Function (PSF) in the J, H, and K band at -100^{o}C and zero ATM pressure are plotted from the Zemax FFT PSF cross-section generated data file (Fig. 5.3). The FWHM of PSFs in J, H and K filters are respectively 39 μm (=2.16 pixel), 51.77 μm (=2.87 pixel) and 70.14 μm(=3.9 pixel) which satisfies Nyquist Criteria in all bands. Polychromatic spot sizes are comparable to the Airy Disc as shown in Fig. 5.4 at -100^{o}C and 0 ATM. Geometrical radii are less than the Airy disc radii (60 μm) at the primary wavelength 1.6 μm over the entire field. FWHM of the spot (Airy Disc) covers 2.8 pixel, which satisfies Nyquist sampling criteria at the primary wavelength. It also satisfies the same criteria in all the filter bands. 80% energy is encircled within 60 μm radius which is the Airy Disc radius at the primary wavelength (Fig. 5.5 at -100^{o}C and 0 ATM). The wavefront irregularities, i.e., Peak to valley and RMS variation are $\approx \lambda/10$ and $\approx \lambda/35.6$ at λ= 1.6 μm respectively (Fig. 5.6 at -100^{o}C and 0 ATM pressure) at the pupil The Modulation Transfer Function (MTF) of incoherent illumination is the modulus of the auto-correlation of the pupil function[108]. Detector MTF is the FT of the detector impulse response function. The impulse response function [h(x,y)] of the detector is a pixel[109]. The impulse response function of the 18 μm square pixel IR detector can be written as,

$$h(x, y) = rect(x/p, y/p) = rect(x/p)rect(y/p) \tag{5.1}$$

TABLE 5.4: Telecentricity (at λ=1.6 μm, P=0 amt and -100°C).

Rectangular Field of View	Angle between chief ray and Optics axis of the system
(0^o, 0^o)	$0.0'$
(0, 0.0084^o)	$29.55'$
(0,-0.0084^o)	$32.06'$
(0.0084^o,0)	$30.73'$
(-0.0084^o,0)	$30.78'$

where p is the pixel size. Detector OTF is,

$$OTF(u,v) = \frac{sin(\pi up)}{(\pi up)}\frac{sin(\pi vp)}{(\pi vp)} \tag{5.2}$$

where u,v are the spatial frequency in both directions. Detector Amplitude MTF is,

$$MTF(u,v) = |\frac{sin(\pi up)}{(\pi up)}||\frac{sin(\pi vp)}{(\pi vp)}| \tag{5.3}$$

This MTF is also useful to verify the Nyquist Criteria. The Pixel size is 18 μm, so the cutoff frequency of the detector is 55.55 cycles/mm [2]. The cutoff frequency of NIR camera is around 27cycle/mm at -100^{o}C and 0 ATM as shown in Fig. 5.7. It is twice the cutoff frequency of the optical system which satisfies the Nyquist Criteria. As per Zemax optical design, the NIR camera PSF is close to the diffraction-limited performance. Under partial AO correction, the PSF at the NIR camera detector consists of two parts. These are the Core and Halo. The core size (FWHM) is $\sim(\lambda/D)$ which is almost same as the diffraction limited disc. The halo size (FWHM) is $\sim (\lambda/D)\sqrt{[1+(D/r)^2]}$ which is almost same as the seeing disc[3]. Our goal is to observe the core of the PSF which will give us enhanced resolution. Thus while designing the optics Nyquist criteria has been satisfied in the Core of the PSF i.e. the Zemax produced PSF. It automatically does the supersampling of the Halo without any aliasing error. The camera design maintains the image space telecentricity to avoid any magnification change at the time of focus readjustment. It also removes the distortion of the system. The chief ray makes zero angle with respect to the optical axis in the case of ideal image space telecentric system. This angle can be used as a metric to quantify the telecentricity of the system and is given in the Table 5.4 at different field of views. The maximum angle at the field position (0, 0.0084°) is $32.06'$ which produces around 4.5% distortion (Fig. 5.8).

[2]Pixel size: 0.018mm, sampling frequency: 1/0.018 cycles/mm.

Broad Band antireflection coating (R<1.5%) at both surfaces of each optical components over the working range 1.1 μm to 2.5 μm are applied. Both dichroics have very good transmission properties. It is almost 96% for science dichroic filter over the 0.9 μm to 2.5 μm. The laser dichroic transmission is also very similar to science dichroic, over 0.380 μm to 2.5 μm as per data sheet. The throughput of the NIR camera is around 76% over the entire wavelength range.

Zemax, OpticStudio's non-sequential (NS) ray tracing mode was used for Ghost light analysis. All the rays are traced first including ghost and the imaging rays are traced first to determine the input power at the detector. Similarly, only the ghost power at the detector is estimated using an appropriate filter which traces only ghost rays from all the components and hit the detector.

The ghost peak power is around 1/1000 times of the input peak power which lies under the sky background level, and hence is negligible.

Tolerance analysis of the NIR camera was to estimate fabrication and alignment tolerance, that is acceptable for maintaining the image quality within an acceptable limit. All the parameter values were randomly changed within specified tolerance constraints and optimized using sensitivity and Monte Carlo analysis in Zemax. Requirements for lens fabrication and alignment accuracy were derived and are listed in Table 5.5.

A sensitivity analysis shows that the change of the RMS spot radius from the nominal RMS spot radius (15.97 μm) is 1.97 μm. The worst offenders in the fabrication and alignments are the radii of curvature of the two surfaces and thickness of the 2nd lens of the collimator, and the distances of components.

Assuming normal distribution statistics, 28000 Monte-Carlo simulations, were performed to see the worst spot. Parameters that were used in the simulation are mentioned in Table 5.5. Table 5.6 shows the results of the simulation, which shows under normal statistics mean RMS spot radius will be 16.02 μm with a standard deviation of 0.85 μm .

5.3 Mechanical Assembly

In this section, we briefly describe the main features of the mechanical assembly of the NIR camera. The NIR camera assembly has three chambers which house

TABLE 5.5: Optics fabrication and alignment accuracy requirement

Name of Parameters	Tolerance
Center thickness	$\pm 0.1mm$
Radius of curvature	$\pm 0.1\%$
Surface tilt	$\pm 0.1^{\circ}$
Surface decenter	$\pm 0.1mm$
Refractive index	± 0.001
Abbe No.	$\pm 1\%$
Center distance	$\pm 0.1mm$
Element tilt	$\pm 0.1^{\circ}$
Element decenter	$\pm 0.1mm$

TABLE 5.6: Monte-Carlo Analysis Result

RMS Spot Radius (μm)	
Nominal	15.97
Worst	19.47
Mean	16.02
Standard deviation	0.85

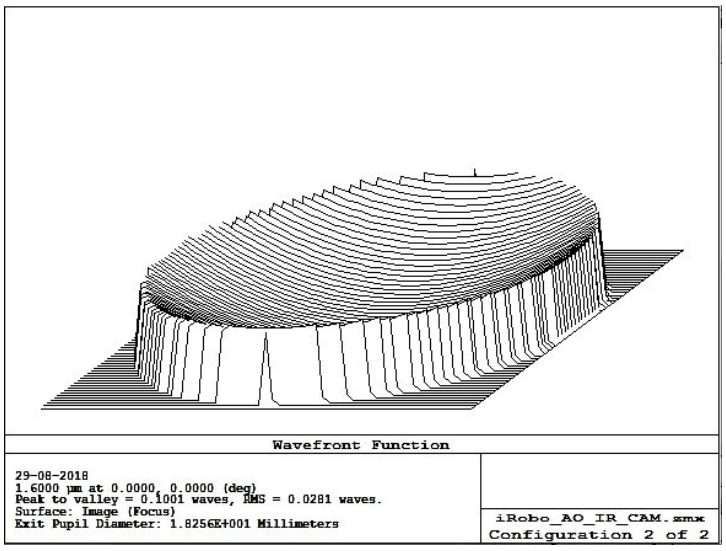

FIGURE 5.6: Wavefront Map: Peak to valley: $\approx \lambda/10$ and RMS variation: $\approx \lambda/35.6$ at λ= 1.6 μm at -100^{o}C and 0 ATM pressure) at the pupil.

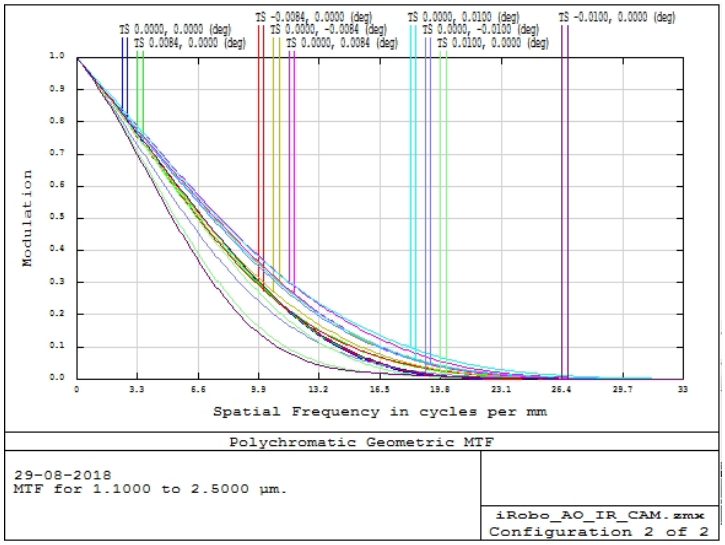

FIGURE 5.7: MTF: Sampling i.e. detector frequency (55.55 cycles/mm) $\approx 2 \times$ cutoff freq. of NIR camera ($\sim$ 27cycle/mm at -100^{o}C and 0 ATM).

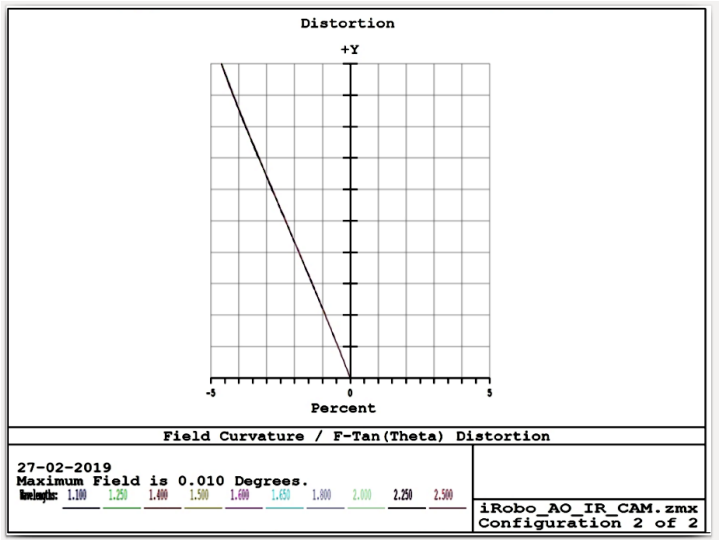

FIGURE 5.8: Distortion: 4.5% distortion at hight field point.

optical components like collimator, filter wheel, camera lens system and the IR detector which are themselves independent subassemblies of their own. The entire NIR camera assembly and a section view of the same are shown in Fig. 5.10 and 5.11 respectively. The optics and optomechanical accessories of weight around 1 Kg are cooled to a temperature of $\approx -100°C$. A radiation shield separates the walls of the chambers from the outside to minimize heat load. The heat load under this configuration is around 0.845 W (refer section 5.4). The radiation shield as well as the collimator and camera assembly holders are well isolated using

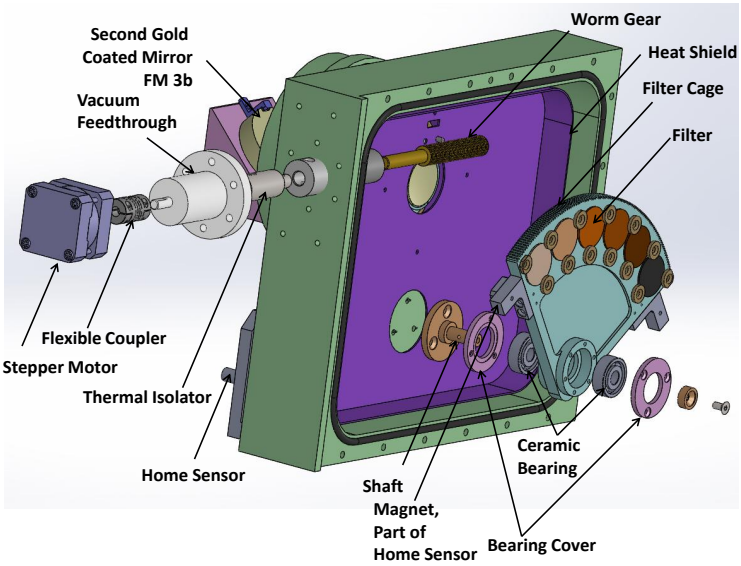

FIGURE 5.9: NIR Camera Filter Wheel Mechanism.

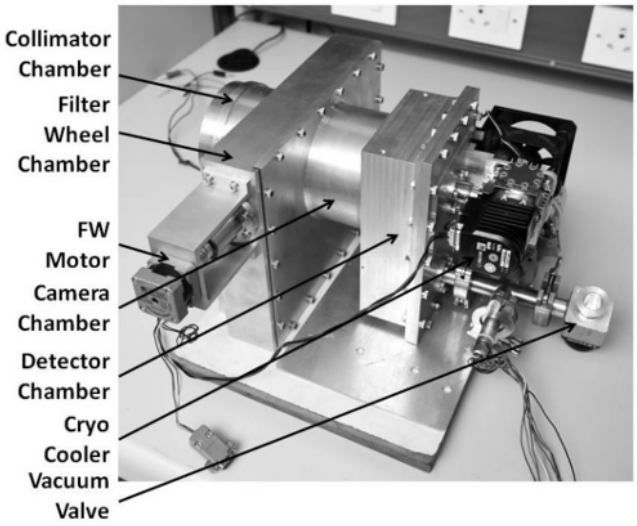

FIGURE 5.10: NIR Camera Mechanical Assembly.

specially designed teflon insulator rings and studs. Flexible copper braids are used to connect the Cryo-cooler's cold tip (Fig. 5.11) to different parts of the system to achieve the desired temperature. The cold stop at the center of which the pupil is located is maintained at a temperature of $-100°C$ by directly connecting it to the cold tip with the help of copper braids.

A compact and light weight 1 W cryocooler is employed for cooling the optics, cold stop and the detector. The cryocooler is already vibration isolated. A provision to introduce extra damping using leaf springs as explained in Gert Raskin 2013

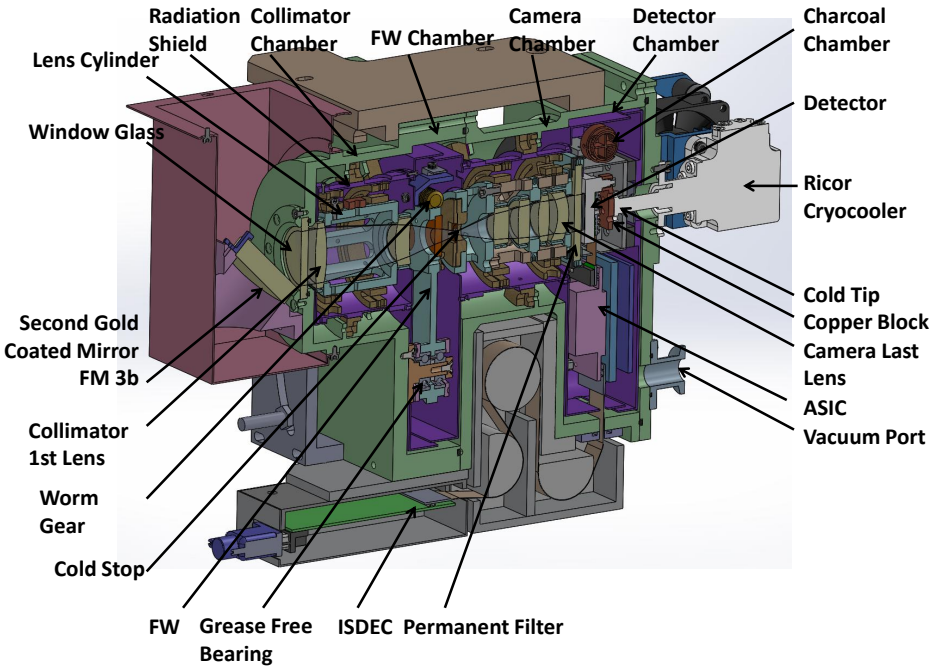

FIGURE 5.11: NIR Camera Section View.

et.al[110] has also been made. The HAWAII[3] detector used for imaging is also directly connected to the cold tip of the cooler with the help of a copper plate sandwiched between them. We have tested and achieved 90 K($-183°$C) at the detector plane as described in section 5.4.1.1.

6061T6 grade Aluminium alloy is used for manufacturing the dewar. All the external mountings were done with the help of stainless steel fasteners. The dewar has a vacuum port and a cooled charcoal chamber mounted inside to minimize effects of degassing from inner surfaces of the dewar and other components.

The filter wheel (FW) is mounted on grease free bearing which has six slots for mounting NIR filters. A Hall sensor is provided for homing the FW. The FW has homing sensors at both ends of the filter mount, which allows for easy homing operation. The pitch of the worm gear is 1.5 mm. A single step of the stepper motor corresponds to 1.8° angle. With a step positioning error of 5%, the overall positioning error in the filter wheel is less than 6.5 μm at the centre of the filter. The filter diameter is 25.4 mm, well above the beam diameter of 9 mm, which eliminates the probability of vignetting.

[3]HgCdTe Astronomical Wide Area Infrared Imager.

All the lenses are mounted on the lens holders with vacuum and cryogenic grade thermally conducting epoxy glue. While assembling and handling the camera's opto-mechanical components adequate precautions against contamination [111] were taken.

Contamination Control Plan: Adequate contamination control is necessary to make low out-gassing of the chamber. The cleaning process can be divided into four steps,

- Preliminary Cleaning: The parts were scrub washed with detergent and cleaned under running water followed by wiping with lint-free tissues. All the cleaned parts are dried under a heating lamp.
- Coarse Cleaning: Then the parts are rinsed with de-mineralized water and further cleaned at temperature 60°C to 70°C in an ultrasonic bathtub. A nylon brush was used to scrub followed by rinsing again with de-mineralized water. Again dried under a lamp on a laminated air flow table.
- Precision Cleaning: The coarse cleaned components were cleaned for 5 minutes in the ultrasonic bathtub with de-mineralized water at temperature 60°C to 70°C. Then these parts were rinsed with de-mineralized water and then dried, followed by rinsing with isopropyl alcohol (IPA) and drying.
- Baking the individual parts: All the elements of IR camera were baked at temperature 80°C over a few hours. The baked items were packed in clean bags for storing in the clean room under dry environment.

The entire process was done in the clean room under laminar clean air flow using clean hand gloves and mask.

5.4 Thermal Analysis

The thermal noise performance of the NIR HAWAII detector is extremely sensitive to temperature. There is blackbody radiation from many parts of the camera as well as the telescope which introduces stray light that can contaminate the image at the detector. The detector needs to be cooled to around liquid nitrogen

TABLE 5.7: Parameters of the heat load calculation.

Parameters	Description
Emissivity of all surfaces ($\varepsilon_1 = \varepsilon_2 = \varepsilon_{3,2} = \varepsilon_{3,1}$)*	0.1
Length of the cylinder (h)	260 mm
Radius of inner cylinder (r_1)	25 mm
Surface area of inner cylinder (A_1)	40840 mm^2
Temperature of inner cylinder (T_1)	173 K
Radius of outer cylinder (r_2)	52 mm
Surface area of outer cylinder (A_2)	84948 mm^2
Temperature of outer cylinder (T_2)	300 K
Radius of shield cylinder (r_3)	39 mm
Surface area of shield cylinder (A_3)	63711 mm^2
View factor between two surfaces (say a and b), $F_{a,b}$	1†

* Emissivity of inner, outer, shield to inner and shield to outer surface are $\varepsilon_1, \varepsilon_2, \varepsilon_{3,1}, \varepsilon_{3,2}$ respectively.
† Here we have taken view factors are 1 in our calculation for the over estimation of the heat load.

temperature while the camera components to a sufficiently low temperature to minimize the effects of the thermal noise and the stray radiation. Theoretical estimation of the heat load is carried out to guide the design of the radiation shield to obtain adequate heat insulation and to find the required wattage of the cryo cooler to achieve the required temperature of the detector and interior camera components. In this section t he power (heat energy per unit time) which flows into the camera system by radiation is estimated, assuming heat transfer by conduction and convection are negligible [4]. The complex mechanical structure is approximated to a simple model, constituted with a dewar body outer cylinder, the inner cylinder, i.e. lens spacer which contains lenses and a cylindrical radiation shield in between the inner and outer cylinder. There is a window glass at one end and the detector at the other end of the dewar. Stephan's Law is applied to this system to determine the radiative heat load. We need the optics and their mounts to be at $\approx$ 173 K (-100°C) and the detector at 77 K (-200°C). The room temperature is taken to be 300 K (27°C) at IGO which is higher than the average night time temperature. The results are approximate (adapting Holman approach [112]); a detailed modelling of the system would be required for a full thermal analysis which is beyond the scope of this work. The values of the relevant parameters that are used in the calculation are given in Table 5.7.

- Radiation through the dewar cylindrical surface without any shield:

[4] All cylinders are thermally insulated with each other and kept at 0 ATM pressure.

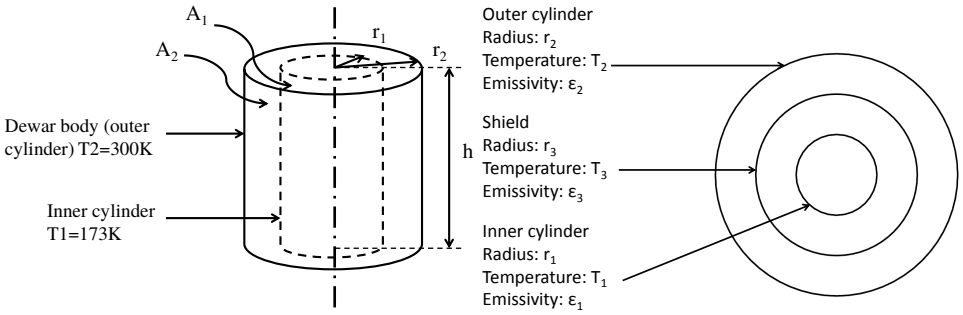

FIGURE 5.12: No radiation Shield in between two cylinder.

FIGURE 5.13: One radiation Shield in between two cylinder.

The net rate of radiation from the outer cylinder (dewar body) to inner cylinder (lens barrel) (Fig. 5.12) without any radiation shield is given by,

$$\frac{dQ}{dt}_{2,1,noshield} = \frac{\sigma(T_2^4 - T_1^4)}{\frac{1-\varepsilon_2}{A_2\varepsilon_2} + \frac{1}{A_2F_{2,1}} + \frac{1-\varepsilon_1}{A_1\varepsilon_1}} = 1.1632\,\mathrm{W} \tag{5.4}$$

where σ is the Stephan - Boltzmann constant.

- Radiation through the dewar cylindrical surface with one shield:

  The net rate of radiation from the outer cylinder (dewar body) to inner cylinder (lens barrel) (Fig. 5.12) with one radiation shield is given by,

$$\begin{aligned}\frac{dQ}{dt}_{2,1} &= \frac{\sigma(T_2^4 - T_1^4)}{\frac{1-\varepsilon_2}{A_2\varepsilon_2} + \frac{1}{A_2F_{2,3}} + \frac{1-\varepsilon_{3,2}}{A_3\varepsilon_{3,2}} + \frac{1-\varepsilon_{3,1}}{A_3\varepsilon_{3,1}} + \frac{1}{A_3F_{3,1}} + \frac{1-\varepsilon_1}{A_1\varepsilon_1}} \\ &= 0.63\,\mathrm{W}\end{aligned} \tag{5.5}$$

  The heat load considering one radiation shield is ≈ 0.63 W for maintaining the temperature of dewar body and inner cylinder respectively at 27°C and ~ -100°C.

- Radiation through the window glass:

  Actual transmission curve of IR grade Fused Silica shows a transmission of $\sim 90\%$ from $1.1\mu m - 3.4\mu$m; from $3.4\mu m - 4.4\mu$m the transmission falls gradually to zero. For simplicity of our calculations we have assumed that beyond 3.4 μm the transmission is zero. The assumed transmittance (τ), emissivity (ε) and reflectivity (ρ) of the dewar window glass which are used

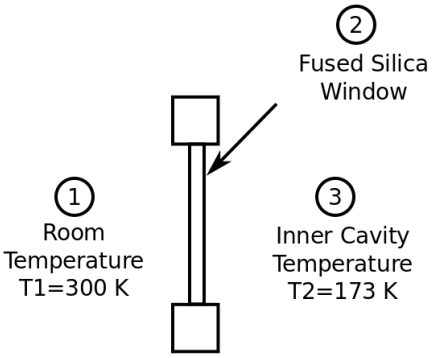

FIGURE 5.14: Schematic diagram of window glass of NIR Camera for calculation of radiation through it.

TABLE 5.8: Radiation energy through window glass of dewar.

Region	Temperature, T(K)	Total Emissive Power $E_b = \sigma T^4$ (watt/m^2)	Wavelength $\lambda(\mu m)$	λT (μm K)	Fraction of Radiation Power (F)*
1 Outside Cavity	T1: 300	E_{b1}: 459	λ_{cutoff_low}:1.1 λ_{cutoff_high}:3.5	330.0 1050	~0 0.0321×10^{-3}
3 Inside Cavity	T3: 173	E_{b3}: 51	λ_{cutoff_low}:1.1 λ_{cutoff_high}:3.5	605.5 190.3	0.173×10^{-7} ~0

* Fraction of total radiation power over wavelength range 0 to λ_{cutoff} taken from Table 8-1 of Heat Transfer by J.L.Holman [112].

in the calculation are given below.

$$1.1\mu m<\lambda<3.5\mu m: \quad \tau = 0.9,\ \varepsilon = 0.1,\ \rho = 0$$
$$\lambda>3.5\mu m: \quad \tau = 0,\ \varepsilon = 0.8,\ \rho = 0.2$$

Total power over the wavelength bands are calculated by consulting Table 8-1, p-382 Heat Transfer by J.L.Holman[112] and Table 5.8 at the both side of the cavity.

Total power over the wavelength band ($1.1\mu m$−3.5 μm) per unit area at the both side of the cavity are given by,

Outside the cavity :

$$E_{b1}(1.1\mu m - 3.5\mu m) = 0.0321 \times 10^{-3} \times E_{b1} = 0.0321 \times 10^{-3} \times 459 \quad (5.6)$$
$$= 0.147\,\text{watt/m}^2$$

Inside the cavity :

$$E_{b3}(1.1\mu m - 3.5\mu m) = 10^{-7} \times E_{b3} = 0.173 \times 10^{-7} \times 51 \approx 0\,\text{watt/m}^2 \tag{5.7}$$

Using Equation 5.6 and 5.7, the net heat flow into the dewar from outside per unit area of the window glass over the band $(1.1\mu m - 3.5\mu m)$ is given by,

$$\begin{aligned} \frac{dQ}{dt} &= \frac{E_{b1}(1.1\mu m - 3.5\mu m) - E_{b3}(1.1\mu m - 3.5\mu m}{R_{eq}} \\ &= \frac{0.147 - 0}{1.0526} = 0.14\,\text{watt/m}^2, \end{aligned} \tag{5.8}$$

where equivalent resistance of the radiation network (R_{eq})[5] is 1.0526 in the said band.

Total power over the wavelength band $(3.5\ \mu m - \infty)$ per unit area at the both side of the cavity are given by,

Outside the cavity :

$$E_{b1}(3.5\mu m - \infty) = [1 - (0.0321 \times 10^{-3})] \times E_{b1} \approx 1 \times 459 = 459\,\text{watt/m}^2 \tag{5.9}$$

Inside the cavity :

$$E_{b1}(3.5\mu m - \infty) = (1 - 10^{-7}) \times E_{b3} \approx 1 \times 51 = 51\,\text{watt/m}^2 \tag{5.10}$$

Using Equation 5.9 and 5.10, the net heat flow into the dewar from outside per unit area of the window glass over the band $(3.5\ \mu m - \infty)$ is given by,

$$\begin{aligned} \frac{dQ}{dt} &= \frac{E_{b1}(3.5\mu m - \infty) - E_{b3}(3.5\mu m - \infty)}{R_{eq}} \\ &= \frac{459 - 51}{2.5} = 163.2\,\text{watt/m}^2, \end{aligned} \tag{5.11}$$

where equivalent resistance of the radiation network (R_{eq})[6] is 2.5 in the said band. The net heat flow into the dewar per unit area of the window glass over the full spectrum (combining Equation 5.8 and 5.11) is 163.34 watt/m^2. Around 0.215 Watt(=163.34 $\times\pi \times 20.5^2 \times 10^{-6}$) radiation enters into the camera through the dewar glass window of radius 20.5 mm.

[5]Estimation was done following example 8-14 of Heat Transfer by J.L.Holman[112].
[6]see footnote 5

It can be observed comparing both Equations 5.4 and 5.5 that one shield can half the heat load. Total heat load with a single radiation shield is $\sim$ 0.845 (=0.63+0.215) Watt [7]. Thus we have made one radiation shield in the mechanical assembly and used a 1 Watt cooler.

5.4.1 Cryogenic

Small and medium sized telescopes often have restrictions on the instrument volume envelope which they can accommodate. A liquid nitrogen Dewar can be bulky and it needs regular human intervention for refilling. This is not conducive for robotic operations. Therefore, a closed cycle cryocooler is used to cool the instrument. As per the thermal analysis, the heat load on the dewar is $\approx$ 0.845 W, hence a Ricor cryocooler[113] of 1 W power is incorporated. Several copper braid connections are used to maintain adequate cooling inside the chamber. The heat transfer from different parts of the camera to the heat sink, by controlling the cross section of the copper braid. It is also essential to have a large contact area between the copper braid and the cooled part. Well polished contact areas with vacuum grade grease applied reduces thermal loss at every contact. Possible water condensation at the window glass due to temperature drop at the outer surface of the window and is avoided by providing a heating resistor network.

5.4.1.1 Cooling Test

Cooling tests have been conducted to check the performance of the cryocooler. In place of the detector, a copper block (Fig. 5.15) is mounted to the detector holder in the detector chamber. Several 1N4148 diodes in reverse bias are used to measure the temperature of the block and different parts of it. A plot of the temperature of the copper block with time is given in Fig. 5.16. A steady state temperature close to 90 K is reached in about 100 minutes.

[7] Total heat load is much lesser than 0.845 Watt as the actual view factors are < 1.

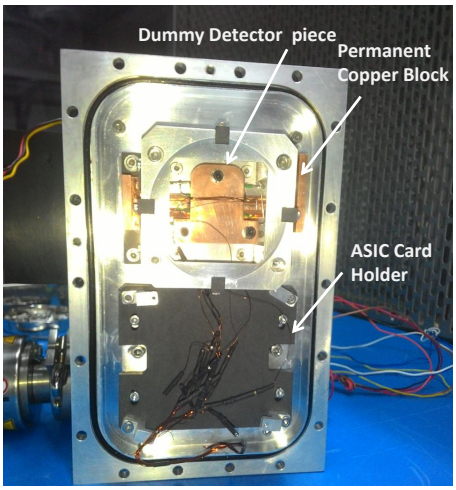

FIGURE 5.15: Dummy Chamber assembly for Cooling test.

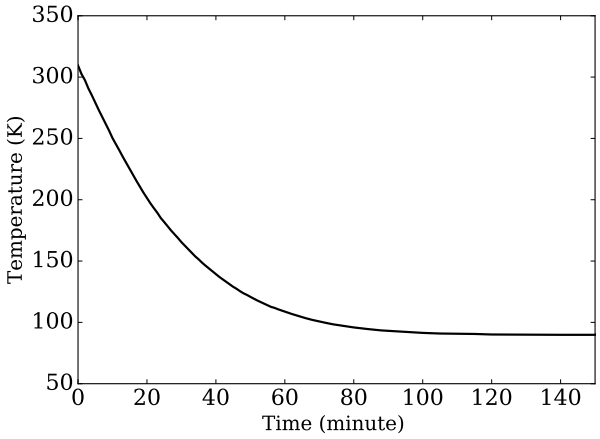

FIGURE 5.16: Cooling test at detector plane with time, steady state temperature $\sim$ 90 K.

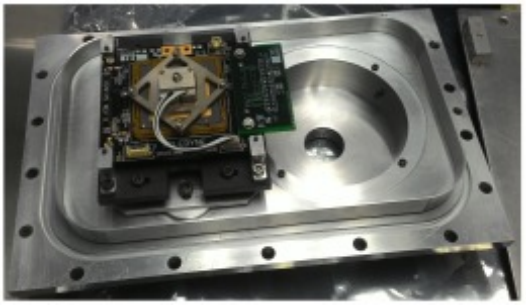

FIGURE 5.17: ASIC is mounted inside the detector chamber.

5.5 Detector Control System

The detector used for imaging is a H2RG device from Teledyne. IUCAA Instrumentation laboratory[114, 115] developed the detector control system and given here for completeness. A cryogenic SIDECAR ASIC card is employed to operate the HAWAII detector. It is placed inside the detector chamber in cold environment (Fig. 5.15, 5.17s). An ISDEC (IUCAA Sidecar Drive Electronics Card) [114] which controls ASIC CARD is placed outside the chamber at normal temperature. ISDEC [114, 115] provides a complete solution to users to carry out detailed characterization of the detector as well as its regular use for astronomical observations. It integrates the camera with Linux based software and other associated firmware and software. ISDECs are completely compatible with both the James Webb Space Telescope ASIC drive electronics (JADE-2) or the SIDECAR Acquisition Module (SAM) board.

5.5.1 Hardware Electronics

ISDEC also allows the specific purpose differential multi-accumulate readout modes which is tuned to do low order wavefront sensing and also H2RG fast strip readout modes (with 16 bit ADC) for high flux high cadence applications. ISDEC-2 [116] can deliver sustained data throughput rates close to 30 MB/sec by using techniques like on-chip data buffering with large FIFOs, and asynchronous USB reads. This technique supports ADC sampling rates (and pixel clocks) from 50 KHz to 500 KHz in all the 1, 4 and 32 output full frame and window readout modes. It supports all the three reset modes (Global Reset, Line by Line Reset and Pixel by Pixel Reset). An identical clock pattern could be used in all three reset modes to keep equal times between the reset and the read phase for all pixels. The entire array or part of the detector could be reset very fast (in few ms) by the Global and Line by Line reset using the unique 'fast reset mode'. As per H2RG array datasheet, 32 or 4 outputs could be used only for full frame readout, but ISDEC supports a mode with which a band or strip of the frame could be readout quickly through 32 outputs. As shown in Fig. 5.18 and Fig. 5.19, the ISDEC-2 board is built around Xilinx make Spartan-3E FPGA. The board's size is about 10cm×10cm. The board generates all the voltages necessary to operate SIDECAR ASIC. The 15 inches long flat, flex cable, feed the voltages to the ASIC. The on-board analogue switches are controlled through software commands to sequence ASIC power. The entire ISDEC can be operated by a single external 5 V power supply, or two separate 5 V power supplies can feed to analogue and digital sections if required. For on-board image processing and buffering purposes, 2 GB NAND flash type memory is employed. The board runs on a 40 MHz onboard clock module, but alternatively to sync with another instrument(s) users can also inject a suitable external clock source through the given SMA connector. The design of the board allows operation at $-40°$C to use within pre-Dewar environments usually found in large instruments.

Apart from standard modes, ISDEC is capable of reading H2RG detector in the following modes

- Strip/band mode (selected region/strip) can be read out higher cadence.
- For low order wavefront correction, special Differential Multi-accumulate mode is developed wherein ISDEC firmware acquires small (4×4, 16×16)

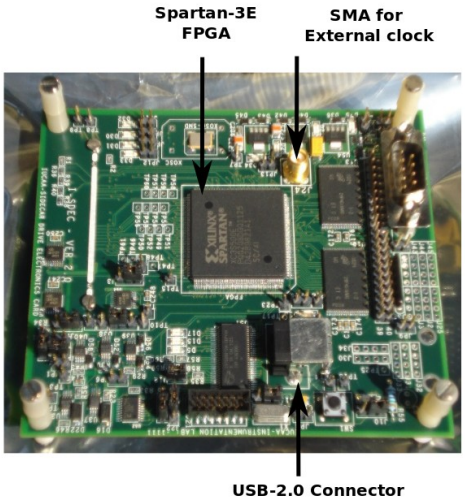

FIGURE 5.18: ISDEC-2 Board Rear view

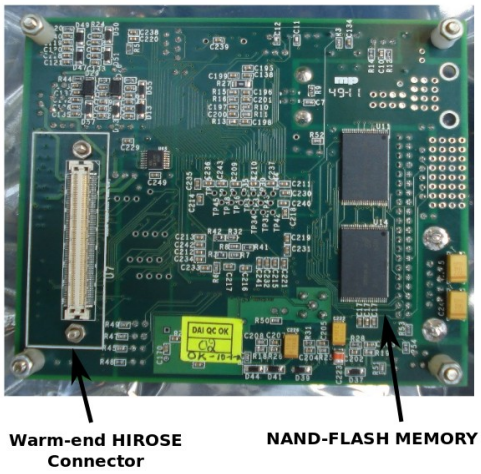

FIGURE 5.19: ISDEC-2 Board Front View

window images at high cadence co-adds the numbers of images and difference between two sets of co-added images are sent to host PC.

Multiple regions (windows) can be read out in an interleaved manner with set periodicity for each window.

We have got 10 - 12 e^- single CDS read noise when measured with bare MUX at 1 e^- / ADU gain in on chip averaged single output window mode with special bias filtering hardware. The detector will be readout under normal operation four output mode with on-chip channel averageing or single output window mode with on chip averaging. The idle mode and continuous reset mode of the frame readout are done at the same frequency. ISDEC does not support Improved Reference Sampling and Subtraction (IRS2) readout mode. However we use special bias filtering hardware to reduce 1/f noise.

5.5.2 System Architecture

The ISDEC system has a very simple layered architecture Fig. 5.20. The topmost is the application layer. It controls the overall operation accepting users input in the form of parameters specified in the parameter files or through a command line interface. The application software further reads the raw image data, strips off the header etc. It also rearranges the data and then creates a multi-extension FITS file. The middle layer (i.e. FPGA firmware) formats the received commands through

a USB slave controller chip commands and then delivers them to the SIDECAR ASIC. This firmware also reads back the ASIC registers as well as image data from ASIC and sends back to the host PC along with appropriate tags/headers. The low-level command protocol and data flow between PC and SIDECAR ASIC are handled and controlled by the FPGA firmware. It computes and appends single bit parity for single word transfers and CRC for block transfers. For programming and configuring SIDECAR ASIC and 16 or 32 bit (CMOS or LVDS) parallel interface, a bidirectional digital serial interface is used to read raw image data from ASIC. The firmware uses the on-chip phase locked loops (PLL) and digital clock modules (DCM) for the operation of the H2RG at different speeds (sampling rates). The ASIC in the bottom layer has the microcontroller program which executes the instructions to operate the H2RG detector in a mode as set and demanded by the above layers. It also writes the raw image data in its internal memory.

Software: The Linux and the C / C++ language are used to develop the ISDEC software. It has various open source libraries (e.g. libusb4, argtable, cfitsio, options, pthreads, etc.) under GPL. The user specified parameters set either as command line arguments or/and through multiple parameter files drives the software which is built as a state machine. The software has separate two programmes. One of them is "Exposure" program which reads the parameters from four parameter files ("Exposure parameter file", "Engineering parameter file", "Reset parameter file" and "Auxiliary parameter file"). The exposure parameter file contains exposure related parameters like the number of resets, number of reads, sampling scheme (Up the Ramp Groups or Fowler Sampling), frame size, etc. The reset parameter file has pre-amp parameters, and array reset schemes. The engineering parameter file handles only engineering level parameters which do not change from one exposure to another exposure like the number of outputs, channel averaging, single / differential output, etc. The auxiliary parameter file deals the additional parameters, i.e. observatory, telescope or instrument specific parameters etc. to include in the header of the FITS as per the wish of the observer. The Exposure program populates the various information (like exact exposure time per frame, time stamps, etc.) in the header of the FITS and produces multi-extension FITS files (one per set of reads called group) The other program is Configure program which powers the ASIC, downloads the microcode into the ASIC, configures the FPGA, fine tunes the detector biases and also has modules for diagnosis / trouble shooting purposes.

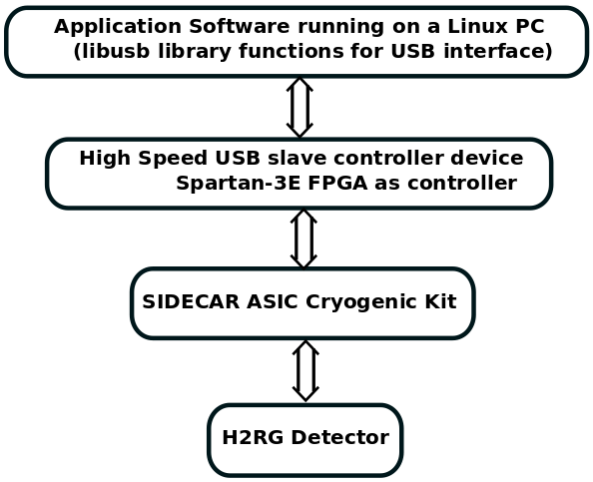

FIGURE 5.20: Tiered view of ISDEC based system